MNE 19 (2023) 100186

Contents lists available at ScienceDirect

Micro and Nano Engineering

journal homepage: www.sciencedirect.com/journal/micro-and-nano-engineering

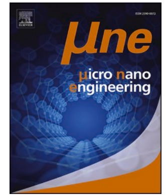

Rapid prototyping of 1xN multifocus gratings via additive direct laser writing

Marie Reischke [a,b,c,1], Oliver Vanderpoorten [a,*,1], Florian Ströhl [a,*]

[a] Department of Physics and Technology, UiT The Arctic University of Norway, Tromsø, Norway
[b] Max Planck Institute for the Science of Light (MPL), Erlangen, Germany
[c] Department of Physics, Friedrich-Alexander-Universität Erlangen-Nürnberg, Erlangen, Germany

ARTICLE INFO

Keywords:
Additive manufacturing
Two-photon
Direct laser writing
Photolithography
3D microscopy
SU-8
Diffraction grating

ABSTRACT

Multifocus gratings (MFGs) enable microscopes and other imaging systems to record entire *Z*-stacks of images in a single camera exposure. The exact grating shape depends on microscope parameters like wavelength and magnification and defines the multiplexing onto a grid of MxN *Z*-slices. To facilitate the swift production and alteration of MFGs for a system and application at hand, we have developed a fabrication protocol that allows manufacturing of 1xN MFGs within hours and without the requirement of clean room facilities or hazardous etching steps. Our approach uses photolithography with a custom-built stage-scanning direct laser writing (DLW) system. By writing MFG grating lines into spin-coated negative tone SU-8 photoresist, polymerized parts are crafted onto the substrate and thus directly become a part of the grating structure. We provide software to generate the required MFG grating line paths, details of the DLW system and fully characterize a manufactured MFG. Our produced MFG is 5.4 mm in diameter and manages to record an image volume with a *Z*-span of over 600 μm without spherical aberrations or noticeable loss of resolution.

1. Introduction

Many biological processes happen in 3D and on small times scales resulting in a need for fast volume acquisition techniques. One route to meet this requirement is multifocus imaging. In multifocus imaging whole image stacks can be acquired instantaneously not requiring any scanning, which has been shown to enable fast volumetric imaging of various biological systems [1–4]. Multifocus imaging entails distributing different *Z*-planes of an image volume onto separate areas on a two-dimensional camera chip. To-date, this has been demonstrated with reflective, refractive, and diffractive optical elements. Cascaded beam splitters introduce different path lengths for different partial reflections resulting in different focus planes [1]. Specially shaped multiplane prisms imprint a defocus onto various multiple partial reflections and thus also provide copies of the beam path with different path lengths when directed onto a camera [2]. In light-field imaging, a microlens array enables recording of the positions and direction of light rays from a nominal image plane, that enable computational reconstructions of the image volume [5]. An image can also be split and refocused using multifocus gratings (MFGs) which imprint a different defocus per diffraction order [4]. A major benefit of prisms, beam splitter cascades and MFGs over light-field microscopy is the preservation of the full numerical aperture (NA) and thus resolution of all image planes. MFGs furthermore stand out as they have been demonstrated with the by far largest number of simultaneous planes. In one implementation up to 25 split planes [3] where shown, while beam splitter cascades [1] and prisms [2] only reached 9 and 8 planes respectively.

Unfortunately, a single MFG is designed for a specific *Z*-spacing, objective, and wavelength, while different biological samples may require different multifocus characteristics, for instance different plane spacing or the use of a different objective. Therefore, a method for rapid prototyping of different MFG designs would highly increase the usability of MFGs in microscopy applications. Production of a large arsenal of MFGs to adopt to different applications at hand requires a fast, easy, and low-cost fabrication protocol. While very flexible prototyping seems possible with spatial light modulators (SLMs) as digital gratings [6–8], optical set-ups with large pupil sizes limit the application of SLMs due to their finite number of pixels. A further side-effect of SLMs are spurious undesired extra-diffraction orders, which may require cumbersome additional advanced post processing techniques [7].

* Corresponding authors.
E-mail addresses: oliver.vanderpoorten@uit.no (O. Vanderpoorten), florian.strohl@uit.no (F. Ströhl).
[1] These authors contributed equally to this work.

https://doi.org/10.1016/j.mne.2023.100186
Received 13 December 2022; Received in revised form 21 March 2023; Accepted 3 April 2023
Available online 5 April 2023
2590-0072/© 2023 The Authors. Published by Elsevier B.V. This is an open access article under the CC BY license (http://creativecommons.org/licenses/by/4.0/).

An established approach for MFG fabrication is the transfer of an optical grating structure onto a glass substrate using conventional photolithography combined with chemical or reactive-ion-etching [9]. Despite its excellent results, this method is rather slow and costly as it imposes additional complexity to the fabrication through the requirement of clean room handling and the necessity of plasma etching protocols. Furthermore, masks for high-resolution photolithography need to be pre-manufactured, which imposes additional delays in time and costs during an empirical development pipeline. Similarly, *E*-beam lithography allows for cutting edge resolution of binary MFG gratings but comes with high facility costs and usage of maintenance-intensive vacuum technologies. Furthermore, limitation exists in terms of realisable heights when approaching the micron range due to low penetration depth of electrons in photoresist. Although this has been largely resolved by proximity effect correction software, which now even allows for grey scale *E*-beam lithography, optical methods compare favourably in MFG production. Latest UV greyscale lithography even facilitates high throughput production of micro-optical components and gratings, which are suitable for rapid prototyping of MFGs with various height levels (non-binary gratings). However, as these systems are investment intense, conventional optics or imaging laboratories may have only limited access to such machinery.

As an avenue to resolve these problems, we have developed a fabrication protocol for binary MFGs on silicon wafers, which uses a custom-built direct laser writing (DLW) system. The protocol can be easily adapted to commercial machines such as maskless aligners or 2-photon lithography systems [10,11] and uses additive manufacturing by direct laser writing. The additive DLW approach is an intriguing possibility for prototyping due to its simplicity and versatility. In particular, the fabrication becomes a single lithography process by using a polymerized photoresist as the optical grating material after development. Our protocol encompasses the design of 1xN gratings, the extraction of pathing data for contour printing, and the processing steps needed for fabrication of these contours via photo-polymerization of spin-coated thin-film SU-8 photoresist on silicon wafers. Contour printing is advantageous over raster printing as it does not require laser power modulation and therefore simplifies the setup even further. With the demonstrated contour printing technique, it is possible to structure large areas of the sample without any stitching artefacts of the pattern.

In short, we demonstrate a rapid prototyping technique for 1xN reflective MFGs, encompassing grating design, pathing, and production via additive direct laser writing. We also provide characterisation of the produced gratings and demonstrate their technological application and performance in a microscopy setup for multifocus imaging without spherical aberrations.

2. Methods

2.1. Design considerations for multifocus grating dimensions

For the design of MFGs a numerical optimization approach from Abrahamsson et al. was used [4]. The algorithm consists of two steps, unit cell design and grating warp. For an optimal efficiency and intensity balance between the orders, a unit cell is designed by a Gerchberg-Saxton algorithm [12]. Upon convergence, a grating unit cell is generated, which forms the basic grating feature and is the building repeating structure of the grating. Warping such an array of unit cells produces the diffraction order dependent defocus effect. The exact warping function is derived from the Abbe-Sine condition and thus realises imaging free of spherical aberrations.

The unit cell generation algorithm requires only the desired number of diffraction orders as input parameter, while grating generation requires the unit cell together with microscope parameters such as magnification, numerical aperture, wavelength, and desired *Z*-distance between adjacent focal planes as inputs [3]. At this point the lithography process can already be started with spin coating a resist layer of appropriate height onto the substrate. The used unit cell generation algorithm provides the grating structure for half-wave phase shifts, which translates into a resist height for a reflective binary grating via an optical path difference of π following the relation $d_{\pi,R} = \frac{\lambda}{4(n_s - n_a)}$. Here, λ is the wavelength, n_s the refractive index of the resist, and n_a the refractive index of air which can be assumed to be $n_a = 1$. The factor of four is due to the light's double pass through the photoresist structure upon reflection at the wafer interface. Given a wavelength of 635 nm (PL202, Thorlabs), a double pass through an SU-8 grating ($n_s = 1.57$) results in a resist height of 278 nm. It can be easier to produce thicker resists. This is possible by adding a 2π phase shift as it does not affect the phase difference. Doing so the height increases to 835 nm, which was easier to fabricate by spin coating on our system and available commonly available photoresists (SPIN150i, Polos).

2.2. Direct laser writing setup

The direct laser writing system is an upright stage-scanning two-photon setup, equipped with a TOPTICA femtosecond laser (785 nm, 80 fs, 80 MHz, external SHG module, FemtoFiber smart 780, Toptica). It is schematically shown in Fig. 1B. The laser's collimated 1.3 mm diameter beam is focused by a 100 × 1.3 NA oil immersion objective (506,008, PL FLUOTAR, Leica) onto the sample, which is mounted on a XYZ piezo stepper stack (ECSz5050–02675,2× ECSx5050–02526, Attocube) controlled by an electrical piezo stage controller (AC100/NUM, Attocube). The XYZ piezo stepper stack enables high-precision long-range translation for the writing process. Two silver-coated mirrors (PF10–03-P01–10, Thorlabs) in kinematic mounts are used for alignment of the laser through the system. Two beam splitters (BS) are used as aids for sample focusing. The lower BS couples light from an LED (Olympus white-LED) into the system, which is used for coarse focusing onto the sample surface. It is removed during the writing process. A small portion of any reflected light from the substrate is directed over the upper BS (T92:R8, CM1-BP108, Thorlabs) through a neutral density filter onto a standard CMOS industrial camera (MER-502-79U3M, Daheng Imaging) for laser focusing.

To facilitate fabrication with DLW a pathing algorithm was developed that converts the calculated grating into pathing coordinates, which are written as lines into the resist by sequentially moving between coordinates with defined speed. The pathing algorithm is specifically designed for 1xN patterns and enables printing of plateaus and thick lines through a concatenation of many lines. The algorithm also supports writing of multiple height layers when using two-photon excitation, which was, however, not used in this work. A custom-written Python software that controls the XYZ stages transfers the contour pattern onto the resist line-by-line. Before starting the writing process, target coordinates can be tilt corrected by measuring the difference between two distant positions on the wafer surface. The integrated optical encoder of the *Z*-piezo stage allows a precise readout and adjustment on the nanoscale (resolution: 1 nm) over a large travel range (8 mm).

2.3. Lithography procedure

The lithographic procedure is divided into five steps, illustrated in Fig. 1A, and follows the photoresist manufacturer's MICROCHEM protocol. (1) SU-8 photoresist (2000.5, MICROCHEM) is spin coated (SPIN150i, Polos) onto the wafer surface and (2) pre-baked on a hotplate at 95 °C for 3 min. The coated wafer is then (3) exposed to the grating pattern on the DLW setup described in 2.2, followed by (4) a post-exposure bake at 95 °C for 5 min. Unexposed areas are dissolved during (5) development of the grating structure in PGMEA for 5 min. Here, exposed lines remain on the wafer surface and the grating is immediately ready to be implemented in the optical system. There are no chemical etching steps involved as the developed photoresist adheres to the wafer surface and forms the optical component. The grating feature

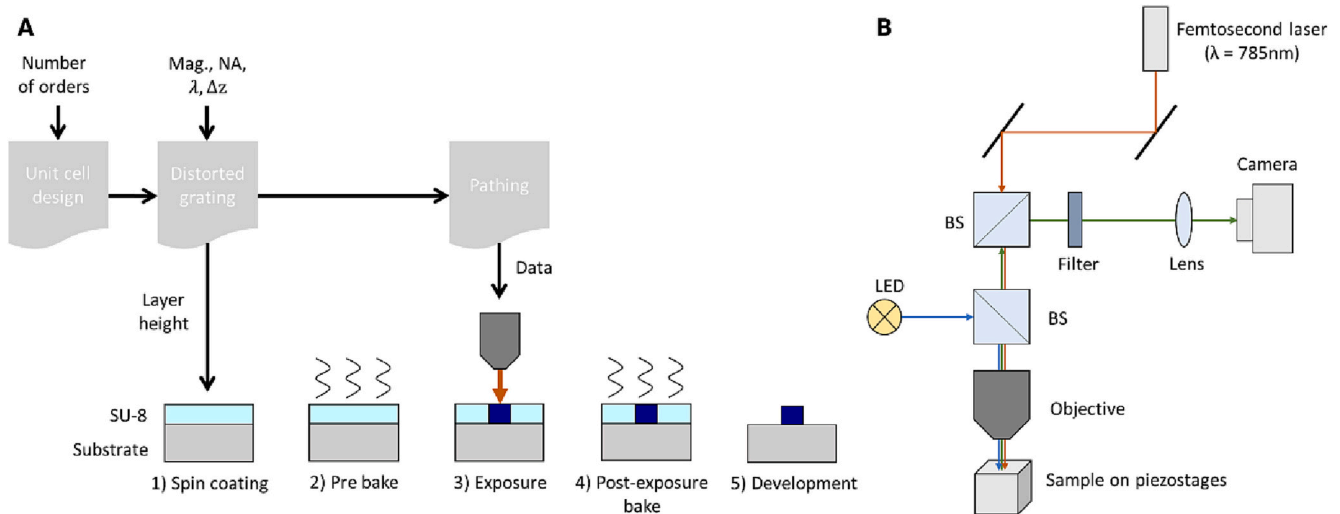

Fig. 1. Fabrication process and setup for rapid prototyping via DLW and negative tone photoresist (e.g. SU-8). A. Schematic overview of the rapid prototyping process. The computational design steps that were implemented in MATLAB with input and output parameters are shown schematically above the fabrication pipeline. Design parameters were used in respective tasks of microfabrication as indicated. SU-8 fabrication involves (1) spin coating, (2) pre-bake, (3) exposure (DLW), (4) post-exposure bake to induce cross linking, and final development (5) using manufacturer-recommended solvents (e.g. PGMEA); B. Schematic of custom-built DLW setup. A laser is focused onto the substrate/resist interface and the sample is moved by a high-precision long-travel piezo stage stack. Focusing onto the surface is facilitated using the back-reflection of the focal spot from the surface at low intensity levels.

height is limited by the layer thickness of the spin-coated photoresist layer, while the grating feature size is dependent on the spot size of the employed focusing objective. Grating dimensions after fabrication were optically inspected using a conventional brightfield/darkfield microscope (Olympus stereoscope) and the grating height measured using a profilometer (KLA Tencor P-6).

2.4. Characterisation of optical grating

To demonstrate the applicability of the grating for 3D microscopy and characterize its optical performance, an optical test setup was built (see Fig. 3A). For illumination a low power 635 nm laser (PL202, Thorlabs) is used. The collimated beam is first expanded with a beam expander (GBE03-A, Thorlabs) and subsequently cropped by a 1 mm diameter pinhole (LCPA1, Thorlabs) to adjust the illuminated field and ensure even illumination. The sample is mounted on a movable mount (SM1ZA, Thorlabs) to change axial position of the object along the optical axis. The mount has a travel range of 2 mm and can be continuously moved with 50 μm per full rotation using a manual micrometre adjuster. An infinity corrected 4× objective (Nikon Plan Fluo) with a nominal NA of 0.13 is used to image the sample in transmission mode. Due to the mounting of the objective its effective NA was reduced to 0.1. After the objective a polarizing beamsplitter (CCM1-PBS251/M, Thorlabs) transmits the linearly polarized light and a subsequent quarter waveplate (AQWP10M-580, Thorlabs) makes it circularly polarized. Two 200 mm focal length lenses (ACT508–200-A-ML, Thorlabs) in 4f configuration relay the pupil plane onto the reflective grating, which is placed in the therefore accessible Fourier plane. The reflected beam travels back through the 4f configuration and the quarter waveplate and is thus reflected by the polarizing beamsplitter. A 200 mm focal length tube lens (TTL-200, Thorlabs) focuses the image onto an sCMOS camera (Prime BSI Express, Teledyne Photometrics).

Three main performance criteria were analysed: the accuracy of the multifocus effect, the intensity balance between the orders, and the prevalence of monochromatic aberrations. For the analysis of the multifocus effect a USAF resolution target was placed in the sample plane and moved axially, spanning the designed *Z*-range of the grating. The intensity balance was investigated quantitatively from the USAF target images using ImageJ. Here, rectangular regions-of-interest (ROIs) the size of bar elements of the USAF chart were selected (elements 3,4, and 5) in each diffraction order and their average intensity value was measured when in focus. The ratio of each order was then compared to the nominal focal plane intensity as mean ratio. Acquisition of a 3D point-spread function (PSF) of 1 μm silica beads (exposure time of 1 ms) allowed the qualitative evaluation of monochromatic aberrations. Starting from the nominal focal plane, the beads were scanned in steps of 25 μm for a total distance of 400 μm in positive as well as negative direction. ROIs of an area where the beads are well visible were manually chosen and aligned.

3. Results and discussion

3.1. Grating properties

To demonstrate the outlined rapid prototyping approach, we fabricated a binary multifocus grating with 1 × 3 diffraction orders. The grating was designed with a centre grating period of $d = 29.3$ μm and a diameter $D = 5.4$ mm. Thus, the grating covers the entire pupil of the objective and displaces the diffraction orders such that three equally sized image planes can be captured side-by-side on the camera. The correct image displacement y_m is calculated via the grating equation: for a laser with wavelength $\lambda = 635$ nm and a tube lens of focal length $f_T = 200$ mm, the first diffraction order $m = 1$ causes a displacement of $y_m = \frac{m\lambda f_T}{d}$ on the camera. The maximum resolution of the objective (0.1 NA) is given by the coherent diffraction limit as $\Delta x = \lambda/NA = 6.35$ μm. A grating height of 0.28 μm would provide a π phase step (see section 2.1), but for simpler handling, we chose a 3π phase step instead. This equals a grating height of 0.84 μm. The focal plane separation, caused through the distortion of the grating is calculated by the grating design software package explained in 2.1 and was chosen to cover ±313 μm. This equals an MFG with an average line thickness of 10 μm at an average spacing of 20 μm. Note that a large focal plane separation via an axial displacement of the camera (as e.g., in beam splitter based multifocus systems) would cause considerable spherical aberrations and therefore a large plane separation is suitable to evaluate the performance of the grating in this respect.

The 5.4 mm diameter grating consists of 184 repeats of the grating unit cell. Assuming a 1 μm lateral voxel size of the DLW system through underfilling its pupil, on average 10 lines per plateau are necessary to

realize the 10 μm thick plateaus. Taking the grating distortion into account, our pathing algorithm calculates a total of 1784 lines to be printed. Using coordinate sampling along each line of one coordinate every 10 μm, the lithography process of the 5.4 mm diameter grating took approx. 6 h to complete using a writing speed of 1000 μm/s of the piezo stepper stages (operating parameters were 35 V and 1000 Hz). The laser power and scanning speed were optimized to obtain reliable polymerization while avoiding burning of the photoresist. We found 78 mW in a focal area of 0.3 μm^2 to be a suitable laser power to ensure this at the given speed. An overview photograph of the produced grating as well as a close-up brightfield microscope image are shown in Fig. 2A and B and individual printed lines are visible in detail under darkfield illumination (Fig. 2C and D).

Profilometer measurements of the fabricated grating (Fig. 2E and F) show a height of 0.71 ± 0.15 μm over the whole grating. Based on the unit cell generation algorithm the efficiency of the produced grating with a height of 700 nm was estimated to be 87% distributed over the three orders with efficiencies of $m_{-1} = 14.6\%$, $m_0 = 57.5\%$, and $m_1 = 14.6\%$. The maximum height of each grating line is 0.86 ± 0.53 μm and is thus close to the designed 0.84 μm grating height. Note that, as the exact spin coating conditions vary depending on the used spin coater and the resist batch, a calibration is generally required to find the optimal spin coating parameters for the available spin coating equipment. The grating lines display a roughness of Ra = 0.08 μm and a large standard deviation, which is presumably due to incomplete fusion of lines and indicative of a smaller-than-expected voxel size of the DLW system. Nevertheless, voxel-lines written near one another fused to plateaus, which represent complete grating lines with measured average

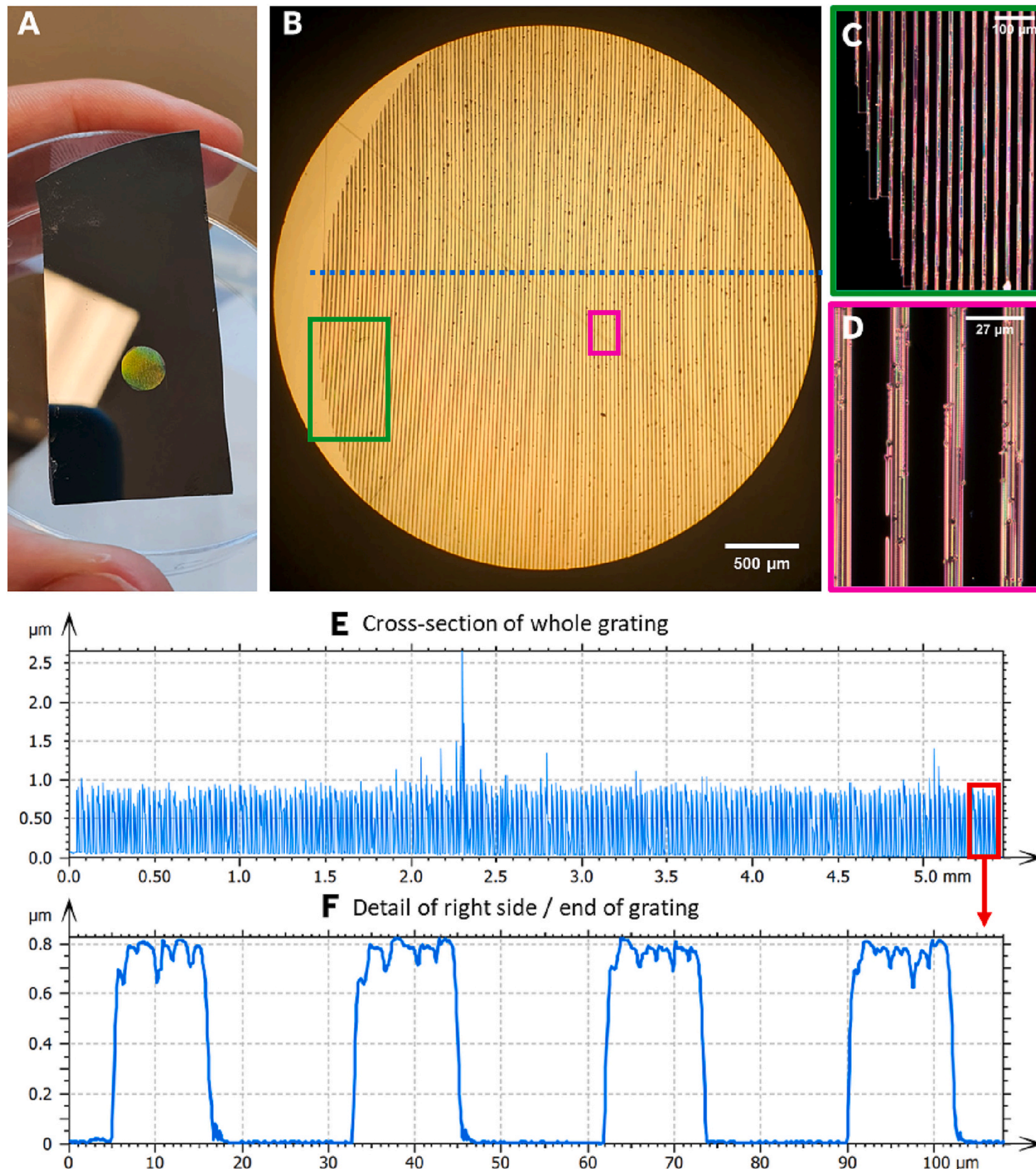

Fig. 2. Fabrication results of the binary reflective multifocus grating. A. Photograph of reflective grating on Si-wafer. B. Brightfield overview of the grating showing the fabricated grating lines. Coloured features indicate details showed in tile C-E. The dashed blue line indicates a cross-section of the grating as shown in E. C. Detail of the edge of the grating imaged with a darkfield microscope. The lines are produced by contour printing. D. Detail from the middle of the grating imaged with a darkfield microscope. The desired line thickness was reached by fusion of lines printed in close proximity. E. Cross-section of the whole grating as measured by a profilometer revealing a constant height of 714 ± 153 nm F. Detailed profile of the grating lines as marked by the red box in tile E revealing a line thickness of 11.89 μm and showing the fusion of lines printed in proximity to reach the design thickness. (For interpretation of the references to colour in this figure legend, the reader is referred to the web version of this article.)

unit cell width of 11.89 μm and a spacing of 17.37 μm. Compared to the unit cell design width, a broadening of 2 μm was observed, while the average unit cell width decreased with a linear slope of −0.014 from left to right which is consistent with the distortion theory. The grating does not contain large defects or impurities, but some small defects occur distributed over the entire grating. These can be attributed to the low laser induced damaged threshold of the photoresist which is an intrinsic material factor that has been previously described [13], but might also be due to temperature diffusion effects while printing.

Note that the broadening of lines does not affect the multifocus effect of the grating but influences the intensity balance. For 1xN gratings, however, grey scale unit cells are found to be without phase jumps (in contrast to MxN unit cells) and thus might indeed benefit from the smoother transitions due to the broadened grating lines.

3.2. Optical performance

Imaging a USAF resolution target with our test setup (Fig. 3A) verified the multifocus functionality of the MFG and sharp images could be acquired in the respective diffraction orders. We find that the focal plane *Z*-spacing is ±0.31 mm as designed (see bottom of Fig. 3B with adjusted brightness and contrast). A comparison between orders shows that the nominal focal plane (i.e., the zeroth order image) receives more light than the ±1 order images. We measure a 4.65 times higher intensity in the nominal focal plane than in the −1 order and a 5.58 times higher intensity than in the +1 order. We attribute the higher intensity in the zeroth order to the height deviation of the grating lines, whereas the small discrepancy between plus and minus first order might stem from (1) adjustment inaccuracies due to the used manual *Z*-translation sample stage, (2) a potential intensity drift of the laser while moving the sample between the two first order images, and (3) a slight decentration of the grating. We furthermore found that small changes in grating height have a large effect on the intensity balance, which proofed challenging to optimize on our spin coater.

The 3D PSF, best visible in the nominal focal plane due to the high intensities, is diffraction limited and symmetrical, but displays astigmatism [14]. Astigmatism might be caused by a slightly misaligned optical element in the test set-up. Otherwise, the axial shape of the PSF is symmetrical, which indicates imaging free of spherical aberrations.

In the ±1 order images the PSF has a similar shape, suggesting that

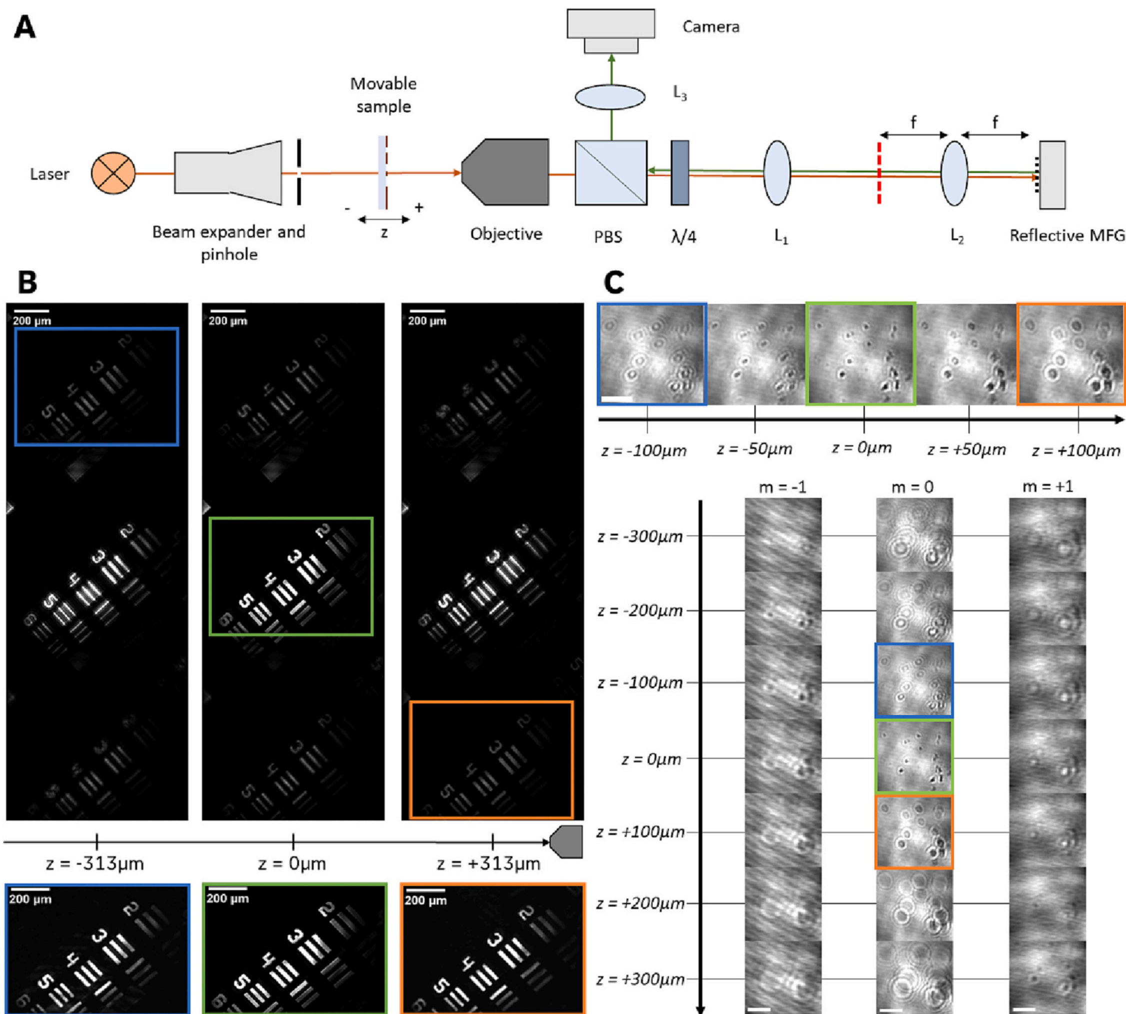

Fig. 3. Evaluation of the optical performance of the grating implemented in a test set-up. A. Schematic image of the test setup used to evaluate the multifocus effect and the intensity balance of the reflective grating that is implemented in a 4f configuration. B. Imaging of a USAF resolution target was used to evaluate the multifocus effect and the intensity balance between the orders. The respective order showed a sharp image when the sample was moved to the design focal plane for the test setup as indicated by the coloured boxes. On the bottom, the order imaging the respective focal plane is shown with individually optimized brightness and contrast. C. Images of the 3D PSF of 1 μm silica beads imaged with the grating implemented in the test setup. The upper montage shows the 3D PSF in the nominal focal plane as imaged by the zeroth order from − 100 μm to 100 μm in steps of 50 μm. The PSF is symmetric with an oval shape stretched at right angle. A combination of 3 montages, each per order and focal plane, is shown below ranging from − 300 μm to 300 μm around the nominal focal plane with steps of 100 μm. The scale bar is 50 μm.

the grating's aberration correction is valid in all imaged focal planes. We measure, however, an enlarged PSF in the ±1 order versus the zero order (FWHM of 6.6 μm and 6.1 μm vs 5.2 μm). We confirmed this finding on the USAF target through decorrelation analysis [15] (7.1 μm and 7.0 μm vs 4.1 μm). Although this deviation might stem from the grating itself, we theorise that the resolution in the ±1 order images might be furthermore impaired due to at least four other factors: (1) vignetting of marginal rays in the objective pupil for defocus images, (2) aberrations in the tube lens upon lateral displacement of the images, (3) measurement inaccuracies due to limited signal and strong interference of stray light in the ±1 order images, (4) decentration of the grating which resulted in a partial occlusion of the parts of the pupil in the ±1 order. Future improvements to the components of the set-up might enable us to pinpoint the decrease in resolution more precisely.

3.3. Further aspects

The overall efficiency and intensity balance of 1xN gratings can be improved by including more height steps and broaden the grating lines to resembling a smoother grating, even close to sinusoidal in the case of a 1 × 3 MFG [16]. One approach to this end is to 3D print single height steps for each unit cell. This is possible with two-photon (2p) DLW, where a confined two-photon illumination focus enables the necessary axial and lateral resolution. Compared to single photon DLW, two-photon lithography offers superior resolution especially in height and ensures that out-of-focus light is not polymerized. A fully automated two-photon setup based on the same three-axis piezo stepper setup as presented here would be quite versatile and provide a good starting point for prototyping. However, additional automation efforts are required with respect to tilt correction, stage control software, and laser power modulations and synchronisation. Another possibility to smoothen out the unit cell profile might be an extended hard bake of structures prototyped with binary DLW after development [17], albeit this approach is much less versatile than 2p DLW and might induce height shrinking of structures depending on materials used.

On the application side another aspect which needs to be mentioned is dispersion: since diffraction is wavelength dependent, MFGs are heavily wavelength dependent and thus induce chromatic aberrations when implemented in a microscope that images broadband signals. Nevertheless, chromatic correction has been demonstrated for MFGs. In the case of 1xN gratings, this was achieved by placing two blazed gratings in front of the MFG [18], while the combination of a blazed grating and a dedicated colour-correction prism behind the MFG [4] was used for chromatically corrected imaging even with MxN gratings.

4. Conclusion

Multifocus gratings enable simultaneous imaging of multiple focal planes without spherical aberrations while preserving the resolution of the microscope. To quickly adapt MFGs to different focal plane spacings, microscope objectives, or new applications a fast design and fabrication protocol is essential. Here we provided a fast and easy method for 1xN grating fabrication based on direct laser writing and demonstrated it by producing a reflective 1 × 3 grating within hours. As the developed resist is part of the grating structure, etching steps are eliminated and time and effort are minimized. Our additive direct laser writing approach does not require any masks and saves time through contour printing of binary structures. The reflective Si-wafer substrate of the MFG eases focusing of DLW setup and provides for a flat surface, suitable for spin-coating of thin layers of SU-8, which strongly adhere to the silicon wafer surface. The optical performance of the produced 5.4 mm diameter grating was evaluated on a test setup and showed multi-plane imaging with a focal plane spacing more than 0.3 mm. If such a MFG were employed in a microscope with a 100× high NA immersion objective, imaging with a focal plane spacing of 500 nm would be possible and would allow for diffraction-limited instant-volume imaging for applications such as 3D particle tracking of intra-cellular organelles. Looking ahead, using the advantageous sectioning of two-photon lithography for direct laser writing would further enhance the capabilities of our approach. High resolution fabrication of non-binary structures would be possible. This would enable fabrication of more complex grating patterns which would optimize the intensity balance between diffraction orders and increase the overall light efficiency even with a larger number of diffraction orders. The current process allows the fabrication of 1xN MFGs. To make full use of size of modern large area camera chips, an expansion to MxN gratings can be beneficial and might be possible through a double exposure of orthogonal Mx1 and 1xN gratings. Nevertheless, a dedicated 2D unit cell shape might deliver superior performance [4], and could be realised through a more complex laser pathing method that includes laser modulation. Producing the gratings on prisms might even enable an intrinsic way to correct for chromatic aberrations. Respective correction measures have been demonstrated and have allowed imaging free of monochromatic as well as chromatic aberrations in fluorescence microscopy [4]. Taken together, the demonstrated additive manufacturing process provides a fast prototyping method of 1xN MFGs that can be easily adjusted to different optical applications such as volumetric imaging or particle tracking.

Author contributions

MR designed the grating, developed the pathing algorithm, built the test setup, and performed characterisation measurements. OV built the lithography setup. FS conceived and supervised the project. MR and OV developed the fabrication protocol. FS and MR analysed the characterisation measurements. All authors contributed to the manuscript.

Declaration of Competing Interest

The authors have no conflicts of interest.

Data availability

Data and software is available at https://doi.org/10.18710/G4NKR7

Acknowledgements

FS acknowledges support by the Norwegian Research Council (#314546) and the publication fund of UiT The Arctic University of Norway. MR acknowledges support by Erasmus+. OV acknowledges funding support from the Norwegian Research Council (#288565) and by the Horizon Europe Framework Programme (HORIZON) (#101064246). The authors want to thank Sara Abrahamsson for helpful discussions about MFGs at an early stage of this project.

References

[1] S. Xiao, H. Gritton, H.-A. Tseng, D. Zemel, X. Han, J. Mertz, High-contrast multifocus microscopy with a single camera and z-splitter prism, Optica 7 (2020) 1477.

[2] A. Descloux, K.S. Grußmayer, E. Bostan, T. Lukes, A. Bouwens, A. Sharipov, S. Geissbuehler, A.L. Mahul-Mellier, H.A. Lashuel, M. Leutenegger, T. Lasser, Combined multi-plane phase retrieval and super-resolution optical fluctuation imaging for 4D cell microscopy, Nat. Photonics 12 (2018) 165–172.

[3] S. Abrahamsson, M. McQuilken, S.B. Mehta, A. Verma, J. Larsch, R. Ilic, R. Heintzmann, C.I. Bargmann, A.S. Gladfelter, R. Oldenbourg, MultiFocus polarization microscope (MF-PolScope) for 3D polarization imaging of up to 25 focal planes simultaneously, Opt. Express 23 (2015) 7734.

[4] S. Abrahamsson, J. Chen, B. Hajj, S. Stallinga, A.Y. Katsov, J. Wisniewski, G. Mizuguchi, P. Soule, F. Mueller, C. Dugast Darzacq, X. Darzacq, C. Wu, C. I. Bargmann, D.A. Agard, M. Dahan, M.G.L. Gustafsson, Fast multicolor 3D imaging using aberration-corrected multifocus microscopy, Nat. Methods 10 (2013) 60–63.

[5] M. Levoy, R. Ng, A. Adams, M. Footer, M. Horowitz, Light field microscopy, ACM Trans. Graph. 25 (2006) 924–934.

[6] W. Lin, D. Wang, Y. Meng, S.-C. Chen, Multi-focus microscope with HiLo algorithm for fast 3-D fluorescent imaging, PLoS One 14 (2019), e0222729.

[7] M.J. Amin, S. Petry, H. Yang, J.W. Shaevitz, Uniform intensity in multifocal microscopy using a spatial light modulator, PLoS One 15 (2020), e0230217.
[8] M.J. Amin, T. Zhao, H. Yang, J.W. Shaevitz, Multicolor multifocal 3D microscopy using in - situ optimization of a spatial light modulator, Sci. Rep. 1–8 (2022).
[9] L. Oudjedi, J. Fiche, S. Abrahamsson, L. Mazenq, A. Lecestre, P. Calmon, A. Cerf, M. Nöllmann, Astigmatic multifocus microscopy enables deep 3D super-resolved imaging, Biomed. Opt. Express 7 (2016) 2163.
[10] A. Dorn, K. Banerjee, P. Rajaeipour, H. Zappe, Çağlar Ataman, Compact refractive objective add-on for adaptive optics microscopy, in: Proc.SPIE 11969, 2022, p. 1196903.
[11] M. Meem, S. Banerji, C. Pies, T. Oberbiermann, A. Majumder, B. Sensale-Rodriguez, R. Menon, Large-area, high-numerical-aperture multi-level diffractive lens via inverse design, Optica 7 (2020) 252.
[12] R.W. Gerchberg, W.O. Saxton, A practical algorithm for the determination of phase from image and diffraction plane pictures, Optik (Stuttg). 35 (1972) 237–246.
[13] E. Kabouraki, V. Melissinaki, A. Yadav, A. Melninkaitis, K. Tourlouki, T. Tachtsidis, N. Kehagias, G.D. Barmparis, D.G. Papazoglou, E. Rafailov, M. Farsari, High laser induced damage threshold photoresists for nano-imprint and 3D multi-photon lithography, Nanophotonics 10 (2021) 3759–3768.
[14] Philip C.D. Hobbs, Building Electro-Optical Systems - Making it all Work, 2nd ed., Wiley, 2009.
[15] A. Descloux, K.S. Grußmayer, A. Radenovic, Parameter-free image resolution estimation based on decorrelation analysis, Nat. Methods 16 (2019) 918–924.
[16] J.W. Goodman, Introduction to Fourier Optics, 2nd ed., McGraw-Hill, 1996.
[17] R.R. Dammel, *Diazonaphthoquinone-Based Resists* (SPIE), 1993.
[18] P. Blanchard, A. Greenaway, Broadband simultaneous multiplane imaging, Opt. Commun. 183 (2000) 29–36.